
Hot-Spot Mix in Ignition-Scale Inertial Confinement Fusion Targets

Inertial confinement fusion (ICF) depends on the formation of a central hot spot with sufficient temperature and areal density for ignition.^{1,2} Laser-driven hohlraums are used to accelerate targets via x-ray ablation^{1,2} at the 192-beam, 351-nm, 1.8-MJ National Ignition Facility (NIF).³ Shock-timing,^{4,5} implosion velocity,⁶ and symmetry^{7,8} experiments on the NIF are underway with ignition-scale targets^{5,9} to optimize the hot-spot formation. The concentric spherical layers of current NIF ignition targets consist of a plastic Ge-doped ablator surrounding a thin shell of cryogenic thermonuclear fuel (i.e., hydrogen isotopes), with fuel vapor filling the interior volume.¹⁰ Liquid deuterium–tritium (DT) is directed inside the ablator shell using a fill tube, and a DT-ice layer is formed using the beta-layering technique.¹¹ As the shell converges, it compresses the fuel vapor, forming a hot spot as it decelerates. The hot spot contains $\sim 20 \mu\text{g}$ of DT mass, which undergoes fusion reactions. As the DT-fusion alpha particles deposit their energy in the hot spot, the hot-spot temperature sharply rises, and a thermonuclear burn wave propagates out through the surrounding cold and dense DT fuel. Ignition is predicted to occur when the temperature and areal density of the hot spot reach a minimum of 5 keV and 0.3 mg/cm^2 , respectively.¹⁰

Radiative and conductive losses from the hot spot can be increased by hydrodynamic instabilities.¹⁰ The Richtmyer–Meshkov and Rayleigh–Taylor hydrodynamic instabilities seeded by high-mode ($50 < \ell < 200$) ablator-surface mass perturbations from intrinsic CH surface roughness, the fill tube, or microscopic dust particles are predicted to mix ablator material into the interior of the shell at the end of the acceleration phase and into the hot spot as it forms (i.e., hot-spot mix), producing Ge K-shell emission.¹² This article presents conclusive experimental evidence of hot-spot mix occurring in ignition-scale implosions, for the first time, and quantifies the amount of hot-spot mix mass. These experimental observations are important for ICF because there is a requirement for ignition, set from multidimensional radiation–hydrodynamic simulations, that the hot-spot mix mass be less than 75 ng (Ref. 10). The amount of hot-spot mix mass, estimated from the Ge K-shell line brightness using a detailed atomic physics

code,¹³ was found to be comparable to the 75-ng allowance for hot-spot mix. Predictions of a simple mix model¹⁴ based on linear growth of the measured surface-mass modulations are close to the experimental results. The strategy to control the amount of hot-spot mix involves reducing the capsule-surface mass perturbations and reducing the growth factors of the hydrodynamic instability¹² of the plastic ablator through dopant and laser pulse shape choices, or changing to another ablator material (e.g., Cu-doped Be).¹⁵

The amount of hot-spot mix mass in ignition-scale NIF implosions was diagnosed using x-ray spectroscopy.¹⁶ The ablator was doped with Ge to minimize preheat of the ablator closest to the DT ice caused by Au M-band emission from the hohlraum x-ray drive.¹⁷ A schematic of an ignition target highlighting the Ge-doped ablator surrounding the cryogenic-DT layer and DT vapor is shown in Fig. 128.1(a). The K-shell line emission from the ionized Ge that has penetrated into the hot spot provides an experimental signature of hot-spot mix.¹² If the Ge remains in the cold and dense ablator, the Ge ionization will be insufficient to create K-shell line radiation; therefore, the Ge K-shell line emission provides a direct diagnosis of Ge-doped plastic mixing with the hot spot.

The Ge emission from DT and tritium–hydrogen–deuterium (THD) cryogenic targets and gas-filled plastic-shell capsules, which replace the cryogenic fuel layer with a mass-equivalent CH layer^{7,8} [shown in Fig. 128.1(b)] was examined. The latter, called a symmetry capsule or symcap, is used to infer the symmetry of the hohlraum x-ray drive by measuring the spatial distribution of the x-ray emission from the hot spot around the time of peak compression under simpler noncryogenically layered conditions. Symcap targets have a D^3He (30:70) gas fill. Ignition targets have an equimolar mixture of D and T; however, tritium-rich layered targets with H and D were imploded to exploit the lower neutron yields for diagnostic purposes.¹⁰ The THD implosions are hydrodynamically equivalent to the DT implosions. As seen in Fig. 128.1, the ignition target had an outside diameter of 2.2 mm and an ablator thickness of $190 \mu\text{m}$. The radial distribution of the Ge-dopant atomic percentage

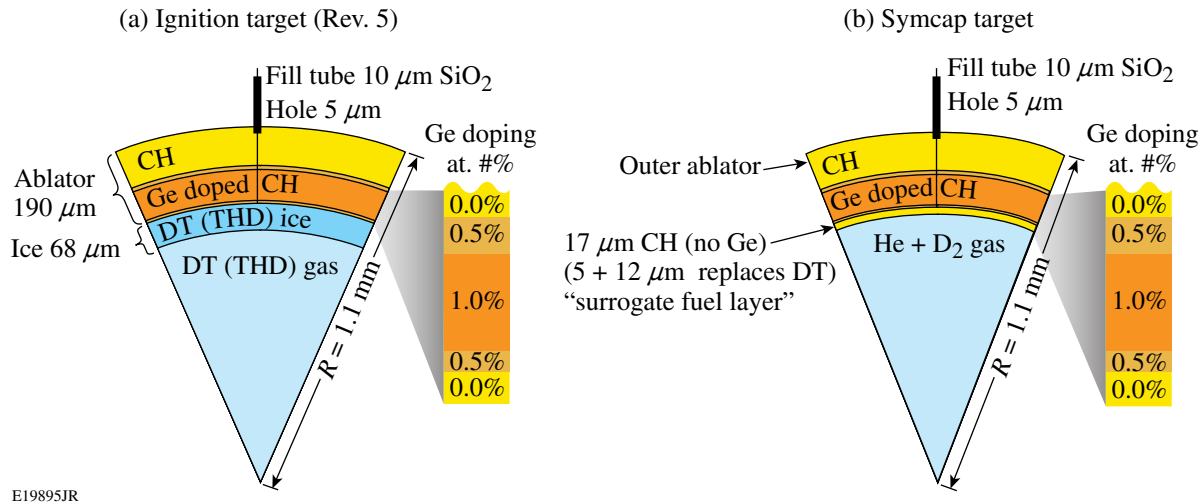


Figure 128.1

Schematic of (a) an ignition target and (b) a symcap target. The cryogenic fuel of the ignition target and the D^3He gas fill of the symcap are transported to the interior of the Ge-doped, plastic ablator using a fill tube. The radial distribution of the Ge atomic doping level in the plastic ablator is shown.

in the plastic ablator was varied to achieve a more-optimal Atwood number between the ablator and the fuel layer at peak shell velocity.¹⁰ In an ignition target the Ge-doped plastic layer is separated from the DT fuel by an undoped plastic layer of $5\text{-}\mu\text{m}$ thickness. In the symcap target, an extra inner $12\text{-}\mu\text{m}$ of plastic of equivalent mass replaces the DT fuel layer.

Bright spots in broadband, gated x-ray implosion images for photon energies greater than 8 keV indicate that hot-spot mix may be occurring in NIF implosions.¹⁸ These bright spots do not provide conclusive evidence, however, of ablator mixing into the hot spot nor do they allow for quantification of the mix mass since the bright spots depend on the plasma composition and conditions and on spatial variations in shell x-ray attenuation caused by regions of low shell areal density. Consequently, a hot-spot x-ray spectrometer (HSXRS) providing coverage in the $9.75\text{- to }13.1\text{-keV}$ range for analysis of the Ge K-shell emission was installed on the NIF.¹⁹ This time-integrated, one-dimensional (1-D) imaging spectrometer viewed the implosion capsule through the laser entrance hole within $\sim 2^\circ$ of the hohlraum symmetry axis. The HSXRS combines a $100\text{-}\mu\text{m}$ -wide slit aperture and a pentaerythritol (PET) Bragg crystal to record 1-D spectral images of the implosion core with a magnification of about 11, a spatial resolution in the target plane of approximately $100\text{ }\mu\text{m}$, and a spectral resolution of 12 eV (Ref. 19). Therefore, the implosion emission is spatially discriminated from the background hohlraum plasma emission in the time-integrated 1-D spectral images. Figure 128.2 shows

an x-ray spectrum measured on symcap implosion N110208 from this diagnostic (black curve), highlighting the spectral features resulting from cold Ge in the pusher (edge drop at 11 keV and fluorescent emission at 9.8 keV) and, most importantly, the emission from the highly ionized Ge in the hot-spot mix mass between 10 and 10.5 keV . He-like Ge is the highest charge state observed. This emission is the first direct evidence of ablator mix into the hot spot of ignition-scale targets. In Fig. 128.2 the x-ray continuum from the hot spot transmitted through the compressed shell is modeled (red curve) assuming the x-ray continuum and the shell optical thickness scale with photon energy ($h\nu$) as $e^{-h\nu/kT}$ and $h\nu^{-3}$, respectively. I_C , M_L , and M_{K+L} are the fitting constants and $h\nu_K$ is the Ge K-edge photon energy.

The Ge K-shell line emission in the $10\text{- to }10.5\text{-keV}$ range from the hot-spot mix mass is highlighted in Fig. 128.3(a) for symcap implosion N110208. As shown in Fig. 128.3(b) a similar spectrum is observed for DT implosion N110620. In these plots the hot-spot x-ray continuum was subtracted and a correction for pusher absorption was applied. This photon-energy range contains a rich spectrum of line emissions from Ge He-like resonance $1s^2\text{-}1s2p(1P)$ and intercombination $1s^2\text{-}1s2p(3P)$ transitions as well as from Ge B-like $1s^2(2s,2p)^3\text{-}1s2p(2s,2p)^3$, Ge Be-like $1s^2(2s,2p)^2\text{-}1s2p(2s,2p)^2$, and Ge Li-like $1s^2(2s,2p)^1\text{-}1s2p(2s,2p)^1$ satellite lines. The spectral envelope of the He_α + satellite feature is sensitive to variations in the electron temperature (T_e) and electron density (n_e) of the mix mass.²⁰

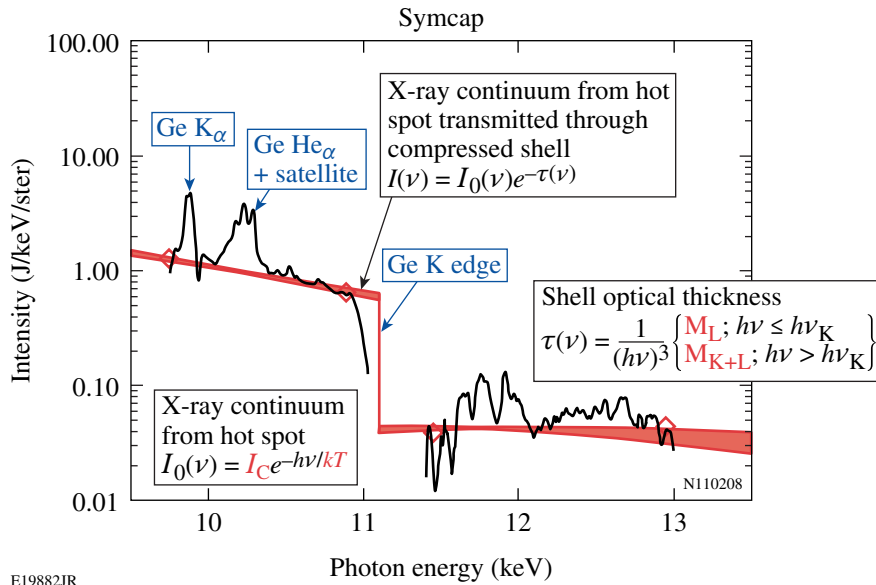
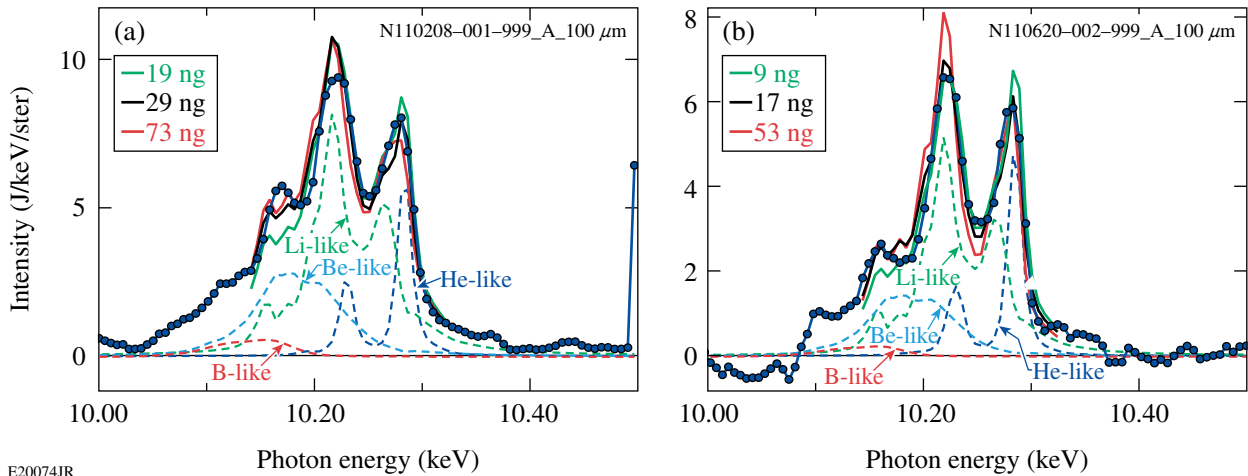


Figure 128.2

Spatially integrated and photometrically calibrated measured x-ray spectrum for symcap implosion N110208 showing Ge He α + satellite and Ge K α emissions and the Ge K edge (black curve). The x-ray continuum from the hot spot transmitted through the compressed shell is modeled (red curve) assuming the x-ray continuum and the shell optical thickness scale with photon energy ($h\nu$) as $e^{-h\nu/kT}$ and $h\nu^{-3}$, respectively. I_C , M_L , and M_{K+L} are the fitting constants and $h\nu_K$ is the Ge K-edge photon energy.

E19882JR



E20074JR

Figure 128.3

Measured Ge K-shell line emission in the 10- to 10.5-keV range from the hot-spot mix mass (blue circles) for (a) symcap implosion N110208 and (b) DT implosion N110620. Modeled spectra assuming uniform plasma conditions and based on least squares fitting are shown [best fit (black curve); 1σ spectral fits (red and green curves)]. Uniform plasma conditions determined from spectral fitting and inferred mix masses are given in Tables 128.I and 128.II. Dashed lines show contributions from He-like, Li-like, Be-like, and B-like charge states for the best fit.

The physical picture of the hot-spot mix is shown in Fig. 128.4. Most of the Ge remains in the compressed shell and absorbs x rays from the hot spot. Depending on the temperature of the shell, this absorption manifests as either Ge K α emission or Ge $1s-2p$ absorption features.²⁰ The ablator material mixed into the hot spot is ionized and emits Ge K-shell x rays. The mix mass is modeled as multiple identical independent spheres of CH ablator mass doped with 1% atomic Ge, each at the same single electron density and temperature, and with

areal densities of Ge-doped CH ($\rho R_{CH\text{ Ge}}$) and Ge (ρR_{Ge}). A detailed atomic and radiation physics model¹³ is used to estimate the amount of mix mass from the Ge K-shell line spectrum as follows: The temperature- and density-dependent emissivity model gives the total emission per Ge mass within the Ge He α + satellite feature. The spectral fit includes self-absorption-coupled level kinetics, giving an estimate of the areal density of Ge in the mix-mass sphere. The Ne through H-like species are represented with detailed-configuration

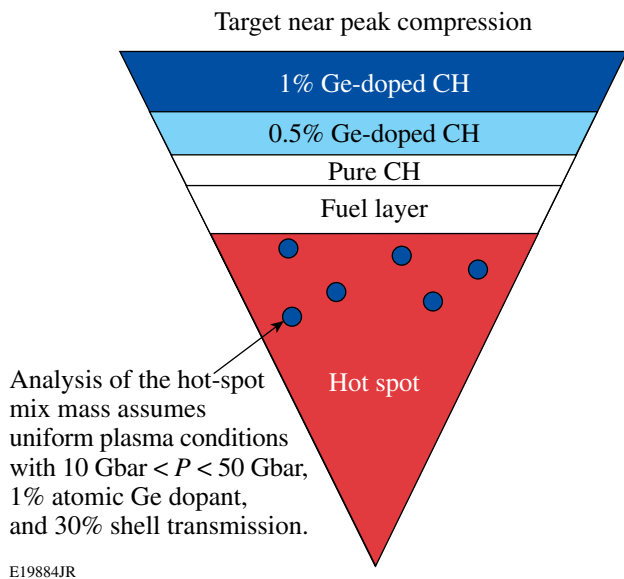


Figure 128.4
Schematic of mix mass in compressed target near peak compression.

accounting (DCA) including all single excitations through $n = 10$, all double excitations through $n = 3$, and splitting important resonance-line-emitting configurations. The Stark-broadening of the Ge line shapes was calculated using the MERL code,²¹ but it is not significant for $n_e < 10^{25} \text{ cm}^{-3}$. The calculated emergent intensity distribution is sensitive to variations in n_e , T_e , and ρR_{Ge} (Ref. 20). The measured spectra are compared with modeled spectra, including instrumental broadening effects for several thousand combinations of n_e , T_e , and ρR_{Ge} , and the best match is determined based on a least squares fit. The amount of mix mass is then determined from the inferred plasma conditions (n_e , T_e , and ρR_{Ge}) and the absolute brightness of the Ge He_α + satellite feature. From the inferred plasma conditions, each sphere of radius R has a CH Ge mass $M_{\text{CH Ge}} = 4\pi R^3 \rho_{\text{CH Ge}}/3$, where $R = \rho R_{\text{CH Ge}}/\rho_{\text{CH Ge}}$ is calculated using the inferred areal densities and electron density of the mix mass and assuming the average ionization is 3.75. The number of spheres the total mix mass are determined by comparing the brightness per sphere to the total measured brightness of the Ge He_α + satellite measurement.

An analysis of the hot-spot mix mass assumes uniform plasma conditions (n_e , T_e , and ρR_{Ge}), electron pressures between 10 and 50 Gbar, 1% atomic Ge dopant, and 30% shell transmission for the Ge He_α + satellite feature (per 1-D hydrodynamic simulations). The estimated shell transmission represents a lower limit for the experiment, leading to an upper limit of inferred mix mass. The two-dimensional (2-D) hydrodynamic simulations show that most of the hot-spot mix mass

originates from the shell layer doped with 1% atomic Ge.¹² The modeled spectra are shown in Fig. 128.3 with the black curve representing the best fit (i.e., minimum χ^2) and the red/green curves representing 1σ spectral fits. The latter define the upper and lower limits of the hot-spot mix mass. The dashed curves in Fig. 128.3 show the contributions to the spectrum from the He-like, Li-like, Be-like, and B-like charge states. Similar mix-mass observations were made on other symcap shots (as shown in Table 128.I) and on DT and THD implosions (as shown in Table 128.II). The mix-mass sphere diameter from the spectral analysis is micron scale, and the number of mix-mass spheres varies from hundreds to thousands, depending on the implosion.

The expected hot-spot mix mass for each capsule is independently estimated with a simple hot-spot mix-mass model that combines linear analysis of the perturbation growth with detailed 2-D hydrodynamic simulations following these steps:¹⁴ (1) transform the capsule-surface perturbation measurements into Legendre-mode space; (2) multiply the decomposed initial perturbations by linear growth factors, calculated for a final perturbation at the ice-ablator interface at peak shell velocity that resulted from a small initial bump on the outside of the ablator; (3) transform back to physical space; (4) find the volume of the ablator that is inside the ice for a DT or THD implosion or the inner CH for a symcap; and (5) multiply by the density calibrated with a detailed bump simulation ($\sim 10 \text{ g/cm}^3$), yielding an estimate of the hot-spot mix mass.¹⁴ The simple hot-spot mix model does not describe the detailed shape of perturbations, but it is calibrated against simulations with actual bump sizes and nonlinear perturbation growth. The hot-spot mix mass (i.e., CH doped with 1% atomic Ge) inferred from the x-ray spectroscopy is compared with the simple hot-spot mix-mass model in Fig. 128.5, and the model is close to the measured results. Most ignition-scale implosions have hot-spot mix mass below the 75-ng requirement for ignition. The experimentally inferred values of hot-spot mix mass in Fig. 128.5 represent a lower bound since the x-ray spectroscopy is only sensitive to the Ge hot-spot mix mass and inferring the CH mass requires an assumed doping level of Ge in the mix mass. Measurements of the mass remaining of ignition-scale targets are close to or slightly larger than predicted, but the implosion velocity is about 10% low.⁶ Higher levels of hot-spot mix mass may occur when higher laser powers and/or thinner shells are used to increase the peak implosion velocity to reach the ignition requirement of $350 \mu\text{m/ns}$ (Ref. 10).

In the future, hot-spot mix will be examined with Cu and Ge dopants located at different radial locations in the ablator to test

Table 128.I: Fitting parameters and hot-spot mix mass inferred for symcap implosions.

Shot	Mix n_e (10^{25} cm $^{-3}$)	Mix T_e (keV)	Mix ρR_{Ge} (mg/cm 2)	CH Ge mix mass (ng)
N101004	0.8 (+0.2, -0.5)	2.4 (+0.6, -0.3)	0.150 (-0, +0.25)	14 (-7, +30)
N110208	1.0 (+0, -0.5)	2.3 (+0.4, -0.3)	0.125 (+0.025, +0.1)	29 (-10, +44)
N110211	0.9 (+0.1, -0.4)	2.0 (+0.3, -0.2)	0.150 (-0, +0.125)	20 (-8, +24)
N110612	0.9 (+0.1, -0.5)	2.2 (+0.5, -0.5)	0.075 (+0.025, -0)	79 (-39, +300)

Table 128.II: Fitting parameters and hot-spot mix mass inferred for DT and THD implosions.

Shot	Mix n_e ($\times 10^{25}$ cm $^{-3}$)	Mix T_e (keV)	Mix ρR_{Ge} (mg/cm 2)	CH Ge mix mass (ng)	
N100929	0.4 (+0.6, +0.1)	1.7 (+0.2, -0.2)	0.075 (+0, -0)	74 (-48, +55)	
N110121	0.3 (+0.6, +0.1)	2.1 (+0.3, -0.5)	0.075 (+0, -0)	67 (-47, +110)	
N110201	1.0 (+0, -0.4)	1.6 (+0.8, -0.5)	0.2 (-0.1, +0.15)	15 (-12, +285)	
N110212	0.5 (+0.1, +0.1)	1.6 (+0.8, -0.5)	0.075 (-0, +0.15)	20 (-17, +265)	
N110603	0.4 (+0.6, +0)	1.9 (+0.6, -0.3)	0.075 (+0.025, -0)	18 (-14, +23)	THD
N110608	0.4 (+0.6, +0)	2.0 (+0.4, -0.3)	0.075 (+0, -0)	63 (-44, +65)	DT
N110615	0.9 (+0, -0.5)	2.2 (+1.0, -0.5)	0.075 (+0, -0)	15 (-10, +56)	
N110620	0.8 (+0.2, -0.5)	2.4 (+0.6, -0.3)	0.075 (+0, -0)	17 (-8, +36)	

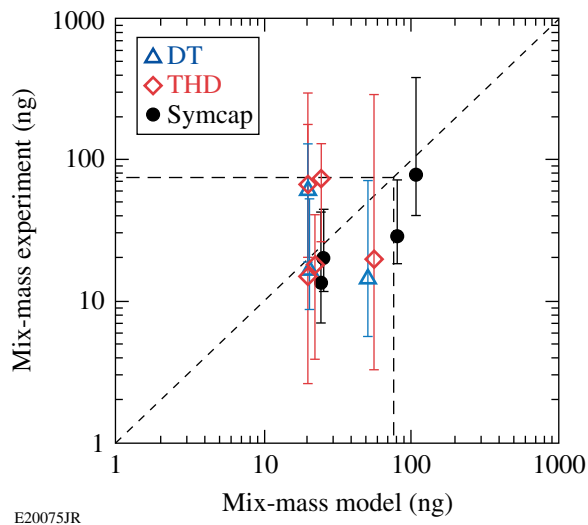


Figure 128.5

Comparison of hot-spot mix mass (i.e., CH doped with 1% atomic Ge) inferred from x-ray spectroscopy with a simple hot-spot mix-mass model that combines linear analysis of the perturbation growth with detailed 2-D hydrodynamic simulations.

assumptions of the origin of the hot-spot mix mass, and x-ray radiography of imposed surface perturbations will be studied to directly relate surface perturbations with the hot-spot mix mass inferred from the x-ray spectroscopy.¹²

Conclusive experimental evidence of the hot-spot mix predicted to occur in ignition-scale implosions as a result of the Richtmyer–Meshkov combined with Rayleigh–Taylor hydrodynamic instabilities¹² has been presented. The amount of hot-spot mix mass in NIF implosions inferred from x-ray spectroscopy is close to or below the 75-ng limit for ignition. These experimental observations are important for ICF because predictions from multidimensional hydrodynamic simulations show that hot-spot mix mass in excess of 75 ng could quench the temperature of the hot spot, reduce the thermonuclear fusion rate, and jeopardize the realization of ignition in the laboratory.¹⁰ Further efforts to control hot-spot mix by reducing the capsule surface-mass perturbations and reducing the growth factors of the hydrodynamic instability of the plastic ablator, or by changing to another ablator material [e.g., Cu-doped Be (Ref. 16)] are ongoing.

ACKNOWLEDGMENT

The authors acknowledge the excellent operation of the National Ignition Facility and helpful suggestions from M. H. Key. This work was supported by the U.S. Department of Energy Office of Inertial Confinement Fusion under Cooperative Agreement No. DE-FC52-08NA28302, the University of Rochester, and the New York State Energy Research and Development Authority. The support of DOE does not constitute an endorsement by DOE of the views expressed in this article.

REFERENCES

1. J. D. Lindl *et al.*, Phys. Plasmas **11**, 339 (2004).
2. S. H. Glenzer *et al.*, Science **327**, 1228 (2010).
3. G. H. Miller, E. I. Moses, and C. R. Wuest, Opt. Eng. **43**, 2841 (2004).
4. T. R. Boehly, D. H. Munro, P. M. Celliers, R. E. Olson, D. G. Hicks, V. N. Goncharov, G. W. Collins, H. F. Robey, S. X. Hu, J. A. Marozas, T. C. Sangster, O. L. Landen, and D. D. Meyerhofer, Phys. Plasmas **16**, 056302 (2009).
5. O. L. Landen, J. Edwards, S. W. Haan, H. F. Robey, J. Milovich, B. K. Spears, S. V. Weber, D. S. Clark, J. D. Lindl, B. J. MacGowan, E. I. Moses, J. Atherton, P. A. Amendt, T. R. Boehly, D. K. Bradley, D. G. Braun, D. A. Callahan, P. M. Celliers, G. W. Collins, E. L. Dewald, L. Divol, J. A. Frenje, S. H. Glenzer, A. Hamza, B. A. Hammel, D. G. Hicks, N. Hoffman, N. Izumi, O. S. Jones, J. D. Kilkenny, R. K. Kirkwood, J. L. Kline, G. A. Kyrala, M. M. Marinak, N. Meezan, D. D. Meyerhofer, P. Michel, D. H. Munro, R. E. Olson, A. Nikroo, S. P. Regan, L. J. Suter, C. A. Thomas, and D. C. Wilson, Phys. Plasmas **18**, 051002 (2011).
6. D. G. Hicks, presented at The Seventh International Conference on Inertial Fusion Sciences and Applications, Bordeaux-Lac, France, 12–16 September 2011.
7. P. Michel *et al.*, Phys. Plasmas **17**, 056305 (2010).
8. G. A. Kyrala *et al.*, Phys. Plasmas **18**, 056307 (2011).
9. M. J. Edwards, J. D. Lindl, B. K. Spears, S. V. Weber, L. J. Atherton, D. L. Bleuel, D. K. Bradley, D. A. Callahan, C. J. Cerjan, D. Clark, G. W. Collins, J. E. Fair, R. J. Fortner, S. H. Glenzer, S. W. Haan, B. A. Hammel, A. V. Hamza, S. P. Hatchett, N. Izumi, B. Jacoby, O. S. Jones, J. A. Koch, B. J. Koziemiński, O. L. Landen, R. A. Lerche, B. J. MacGowan, A. J. MacKinnon, E. R. Mapoles, M. M. Marinak, M. Moran, E. I. Moses, D. H. Munro, D. H. Schneider, S. M. Sepke, D. A. Shaughnessy, P. T. Springer, R. Tommasini, L. Bernstein, W. Stoeffl, R. Betti, T. R. Boehly, T. C. Sangster, V. Yu. Glebov, P. W. McKenty, S. P. Regan, D. H. Edgell, J. P. Knauer, C. Stoeckl, D. R. Harding, S. Batha, G. Grim, H. W. Herrmann, G. Kyrala, M. Wilke, D. C. Wilson, J. Frenje, R. Petrasso, K. Moreno, H. Huang, K. C. Chen, E. Giraldez, J. D. Kilkenny, M. Mauldin, N. Hein, M. Hoppe, A. Nikroo, and R. J. Leeper, Phys. Plasmas **18**, 051003 (2011).
10. S. W. Haan, J. D. Lindl, D. A. Callahan, D. S. Clark, J. D. Salmonson, B. A. Hammel, L. J. Atherton, R. C. Cook, M. J. Edwards, S. Glenzer, A. V. Hamza, S. P. Hatchett, M. C. Herrmann, D. E. Hinkel, D. D. Ho, H. Huang, O. S. Jones, J. Kline, G. Kyrala, O. L. Landen, B. J. MacGowan, M. M. Marinak, D. D. Meyerhofer, J. L. Milovich, K. A. Moreno, E. I. Moses, D. H. Munro, A. Nikroo, R. E. Olson, K. Peterson, S. M. Pollaine, J. E. Ralph, H. F. Robey, B. K. Spears, P. T. Springer, L. J. Suter, C. A. Thomas, R. P. Town, R. Vesey, S. V. Weber, H. L. Wilkens, and D. C. Wilson, Phys. Plasmas **18**, 051001 (2011).
11. A. J. Martin, R. J. Simms, and R. B. Jacobs, J. Vac. Sci. Technol. A **6**, 1885 (1988); B. J. Koziemiński *et al.*, Fusion Sci. Technol. **59**, 14 (2011).
12. B. A. Hammel *et al.*, High Energy Density Phys. **6**, 171 (2010); B. A. Hammel, H. A. Scott, S. P. Regan, C. Cerjan, D. S. Clark, M. J. Edwards, R. Epstein, S. H. Glenzer, S. W. Haan, N. Izumi, J. A. Koch, G. A. Kyrala, O. L. Landen, S. H. Langer, K. Peterson, V. A. Smalyuk, L. J. Suter, and D. C. Wilson, Phys. Plasmas **18**, 056310 (2011).
13. J. J. MacFarlane *et al.*, High Energy Density Phys. **3**, 181 (2007).
14. J. Ralph *et al.*, Bull. Am. Phys. Soc. **55**, 294 (2010).
15. P. A. Bradley and D. C. Wilson, Bull. Am. Phys. Soc. **41**, 1557 (1996); P. Bradley and D. C. Wilson, Phys. Plasmas **8**, 3724 (2001).
16. H. R. Griem, *Principles of Plasma Spectroscopy* (Cambridge University Press, Cambridge, England, 1997).
17. D. S. Clark *et al.*, Phys. Plasmas **17**, 052703 (2010).
18. G. A. Kyrala *et al.*, Rev. Sci. Instrum. **81**, 10E316 (2010).
19. S. P. Regan, B. A. Hammel, R. Prasad, L. J. Suter, P. Bell, M. Eckart, M. A. Barrios, D. K. Bradley, N. Izumi, J. D. Kilkenny, J. L. Kline, G. A. Kyrala, O. L. Landen, T. Ma, R. L. McCrory, D. D. Meyerhofer, T. C. Sangster, and H. Scott, “Hot-Spot X-Ray Spectrometer for the National Ignition Facility,” to be submitted to Review of Scientific Instruments.
20. S. P. Regan, R. Epstein, B. A. Hammel, L. J. Suter, J. Ralph, H. Scott, M. A. Barrios, D. K. Bradley, D. A. Callahan, G. W. Collins, S. Dixit, M. J. Edwards, D. R. Farley, S. H. Glenzer, I. E. Golovkin, S. W. Haan, A. Hamza, D. G. Hicks, N. Izumi, J. D. Kilkenny, J. L. Kline, G. A. Kyrala, O. L. Landen, T. Ma, J. J. MacFarlane, A. J. MacKinnon, R. C. Mancini, F. J. Marshall, R. L. McCrory, N. B. Meezan, D. D. Meyerhofer, A. Nikroo, K. J. Peterson, T. C. Sangster, P. Springer, and R. P. J. Town, “Diagnosing Implosions at the National Ignition Facility with X-Ray Spectroscopy,” to be published in the *AIP Proceedings on the 17th International Conference on Atomic Processes in Plasmas*.
21. R. C. Mancini *et al.*, Comput. Phys. Commun. **63**, 314 (1991).